ELSEVIER

Journal of Organometallic Chemistry 487 (1995) 77–88

Journal of Organometallic Chemistry

The effects of an interannular bridge on the electronic structure of ferrocenium cations

Teng-Yuan Dong *, Shu-Hwei Lee

Department of Chemistry, National Sun Yat-sen University, Kaohsuing, Taiwan

Received 20 April 1994; in revised form 29 June 1994

Abstract

Minor perturbations caused by the interannular trimethylene bridges in a series of ferrocenium cations have pronounced effects on the electronic structure. The X-ray structure of 1,1′:3,3′-bis(propane-1,3-diyl)ferrocenium triiodide has been determined at 298 K: monoclinic, $C2/c$, $a = 11.110(2)$ Å, $b = 9.372(2)$ Å, $c = 18.003(2)$ Å, $\beta = 107.294(9)°$, $Z = 4$, $D_{calc} = 2.401$ g cm^{-1}, $R_F = 0.033$, and $R_{wF} = 0.040$. Compound 1,1′:2,2′-bis(propane-1,3-diyl)ferrocenium triiodide crystallizes in orthorhombic space group $Pnma$ with four molecules in a unit cell with dimensions $a = 8.699(1)$ Å, $b = 13.461(2)$ Å, $c = 15.747(3)$ Å; $R_F = 0.041$, $R_{wF} = 0.042$. The compound 1,1′:2,2′:4,4′-tri(propane-1,3-diyl)ferrocenium triiodide crystallizes in orthorhombic space group $Cmca$ with sixteen molecules in a unit cell with dimensions $a = 18.456(4)$ Å, $b = 33.401(7)$ Å, and $c = 13.470(5)$ Å. The final discrepancy factors are $R_F = 0.077$, and $R_{wF} = 0.090$. An unusually large quadrupole splitting ($\Delta E_Q = 0.936$ mm s^{-1}) is seen in the Mössbauer spectrum of 1,1′:2,2′-bis(propane-1,3-diyl)ferrocenium triiodide at 300 K. We suggest that the larger ΔE_Q value is mainly a result of the metal non-bonding orbitals ($d_{x^2-y^2}$, d_{xy}) starting to interact with the ligand π orbitals as the Cp rings are bent back. The magnetic susceptibility measurements indicate that the electronic ground state for the interannular trimethylene bridge ferrocenium cations is $^2E_{2g}$. The visible absorption spectra of the various ferrocenium cations show a low-energy ligand-to-metal $^2E_{2g} \rightarrow {}^2E_{1u}$ charge-transfer transition. In the case of 1,1′:2,2′:4,4′-tri(propane-1,3-diyl)ferrocenium triiodide, a vibrational structure was observed for this charge-transfer transition at room temperature.

Keywords: Ferrocenium; Iron metallocene

1. Introduction

The discovery of ferrocene set the stage for the synthesis of a vast and continually growing array of structurally diverse complex organometallics. The elucidation of the electronic structure of ferrocene and its simplest derivative ferrocenium ion has been a matter of great interest. Spectroscopic measurements are powerful techniques for checking the electronic structures of these two species. The electronic ground state of ferrocene is a singlet, $^1A_{1g}$ ($e_{2g}{}^4a_{1g}{}^2$), where the one-electron molecular orbitals are predominantly d orbitals in character: $a_{1g}(d_{z^2})$ and $e_{2g}(d_{x^2-y^2}, d_{xy})$ [1]. As indicated by magnetic susceptibility [2] and EPR [3–5] measurements, the electronic ground state of ferrocenium is a doublet, $^2E_{2g}$ ($a_{1g}{}^2e_{2g}{}^3$). On the theoretical side [6], the MO calculations in general indicate that the highest occupied orbitals of ferrocene are a_{1g} and e_{2g}, with the lowest unoccupied level being e_{1g}.

Model compounds **1–5** (Scheme 1) are of use in understanding the influence of Cp-ring tilting on the electronic structure. A recent interesting finding is that there is a significant influence on the electron-transfer rate in the mixed-valence biferrocenium salts **6–8** when the Cp rings in each ferrocenyl moiety are linked by an interannular trimethylene bridge [7–9]. The Mössbauer results indicate that compound **6** is delocalized on the Mössbauer timescale above 77 K [7,8]. Only a single "average-valence" doublet is seen from 77 K to 300 K. The value of the quadrupole splitting ($\Delta E_Q = 1.614$ mm s^{-1}) at 77 K could indicate that there is a strong interaction between the d-manifolds on the iron ion and Cp rings. We proposed that such a structural modification of the parallel relation between the two

* Corresponding author.

SSDI 0022-328X(94)05083-N

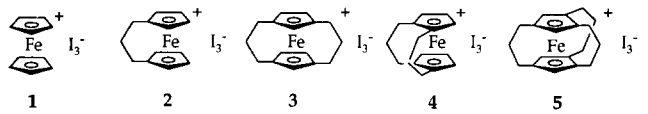

1 2 3 4 5

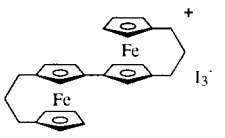

6

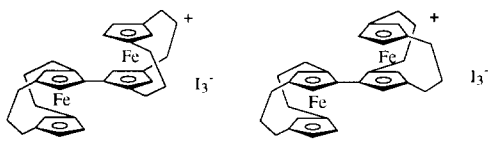

7 8

Scheme 1.

Cp rings around the Fe ion in **6** would lead to greater metal-ligand interactions as rings tilt. The Mössbauer results indicate that compounds **7** and **8** are localized on the Mössbauer timescale (approximately 10^7 s^{-1}) in the solid state at 300 K [9]. At temperature below 300 K, the cations of **7** and **8** show two doublets in the ^{57}Fe Mössbauer spectra, one representing the Fe(II) site and the other the Fe(III) site. The difference in electron transfer rate between **6** and **8** is mainly a result of the difference of coplanarity of the two Cp rings in the fulvalenide ligand. The single X-ray determination of **8** indicates that the two Cp rings in the fulvalenide ligand are not coplanar with a dihedral angle of 42.0(5)° [9]. In **8** the π interactions between the two ferrocenyl moieties are destroyed because the linking bond of the two ferrocenyl units is twisted. There is still one important question that remains. The Mössbauer results indicate that the ferrocenium moiety in **7** and **8** has an unusually large quadrupole splitting of approximately 1.37 mm s^{-1}. In general, ferrocenyl groups (electronic ground state $^1A_{1g}$) give spectra characterized by large quadrupole splitting in the range of about 2.0–2.2 mm s^{-1}, while the spectra of the ferrocenium cations (electronic ground state $^2E_{2g}$) are characterized by small or vanishing quadrupole splitting [10]. To explain the unusually large quadrupole splitting observed for compounds **7** and **8**, we have prepared a series of model compounds **1–5**.

In this paper, the results of ^{57}Fe Mössbauer, magnetic susceptibility and electronic absorption measurements are presented. Furthermore, the unusual physical properties of **1–5** are explained in terms of structural characteristics.

2. Experimental details

2.1. General methods

All manipulations involving air-sensitive materials were carried out by using standard Schlenk techniques under an atmosphere of N_2. Chromatography was performed on neutral alumina (Merck activity II), eluting with hexane-ethylacetate. Dichloromethane and diethyl ether were dried over P_2O_5 and Na/benzophenone, respectively. A sample of 1,1′:2,2′-bis(propane-1,3-diyl)ferrocene was prepared according to the literature procedure [11] and identified by melting point, NMR, and mass spectrum.

2.2. General procedure of acryloylation

The standard method given below is a modification of the procedure of Turbit and Watts [12]. The acryloylating reagent was prepared according to the Friedel-Crafts synthesis by mixing acryloyl chloride (0.78 ml, 9.65 mmol) and excess $AlCl_3$ in 50 mL dry CH_2Cl_2 for 20 min at 0°C under N_2. The excess $AlCl_3$ was filtered out with glass wool.

The acryloylating reagent was added by means of a dropping funnel over a period of 1 h to a solution of corresponding ferrocene (8 mmol) in 80 mL of dry CH_2Cl_2 at −78°C. The reaction mixture was stirred for 18 h at −78°C. The resulting mixture was separated after the reduction of ferrocenium ions with aqueous $Na_2S_2O_3$. The organic layer was washed with saturated aqueous Na_2HCO_3 and water, and it was then dried over $MgSO_4$. The solvent was removed under reduced pressure. The red residue was chromatographed.

2.3. General procedure of reduction

The reduction was carried out by carefully adding, with stirring, small portions of $AlCl_3$ to a mixture of keto-ferrocene and $LiAlH_4$ in dry ether. After 40 min, the solution became yellow, an excess of H_2O was added to it, and the ether layer was separated. The ether layer was washed with water and dried over $MgSO_4$. After the evaporation of the solvent, the crude product was chromatographed.

2.4. Compounds 9, 11, and 13

As shown in Scheme 2, compounds **9**, **11**, and **13** were prepared by following the general procedure of acryloylation. For the ^1H NMR spectra of **9** and **11**,

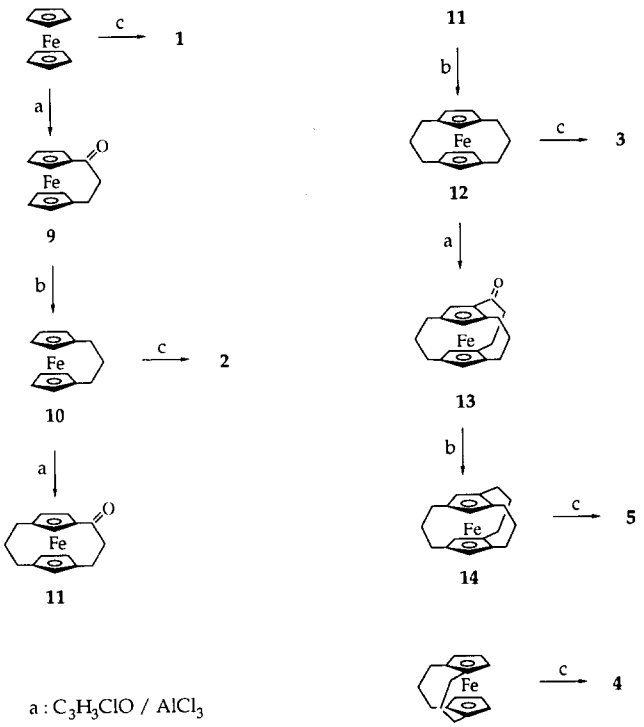

Scheme 2.

one should refer to the original works of Watts and coworkers [12,13]. The properties of **13** are as follows: ^{1}H NMR ($CDCl_3$, ppm): 1.6–2.4 (m, 13H), 2.7 (m, 2H), 3.17 (dt, 1H), 3.69 (d, 1H), 4.00 (d, 1H), 4.50 (d, 1H), 4.65 (d, 1H). Mass spectrum M^+ at m/z 320.

2.5. Compounds 10, 12, and 14

Compounds were prepared by following the general procedure of reduction and identified by ^{1}H NMR and mass spectra. The ^{1}H NMR spectra of **10** and **12** were reported by Watts and coworkers [12,13]. The physical properties of **14** are as follows: ^{1}H NMR ($CDCl_3$, ppm): 1.4 (m, 6H), 1.8 (b, 6H), 2.1 (m, 6H), 3.7 (s, 4H). Mass spectrum: M^+ at m/z 306.

2.6. Triiodide salts 1–5

Samples of **1–5** were prepared by oxidizing the corresponding neutral ferrocene in 1:1 benzene: hexane solution with stoichiometric amounts of I_2 in benzene. The dark microcrystals were collected by filtration and washed with hexane. Anal. Calc. for **1** ($C_{10}H_{10}FeI_3$): C, 21.19; H, 1.78%. Found: C, 21.30; H, 1.82%. Anal. Calc. for **2** ($C_{13}H_{14}FeI_{11/3}$): C, 22.58; H, 2.04%. Found: C, 22.58; H, 2.13%. Anal. Calc. for **3** ($C_{16}H_{18}FeI_3$): C, 29.71; H, 2.80%. Found: C, 29.56; H, 2.66%. Anal. Calc. for **4** ($C_{16}H_{18}FeI_3$): C, 29.71; H, 2.80%. Found: C, 29.05; H, 2.65%. Anal. Calc. for **5** ($C_{19}H_{22}FeI_3$): C, 33.22; H, 3.23. Found: C, 32.54; H, 3.04%.

2.7. Physical methods

The ^{57}Fe Mössbauer spectra were run on a constant-acceleration instrument which has been previously described [14]. Velocity calibrations were made using a 99.99% pure 10 μm iron foil. Typical line widths for three pairs of iron lines fell in the approximate range 0.25–0.28 mm s^{-1}. The isomer shifts are given relative to iron foil at 300 K with no second-order Doppler effects. It should be noted that the isomer shifts illustrated in the figures are plotted as experimentally obtained. Tabulated data are provided.

^{1}H NMR spectra were obtained on a Bruker MSL 200 spectrometer. Mass spectra were obtained with a VG system, model 70-250 S. UV spectra were obtained with a Perkin-Elmer Lambda 9 spectrophotometer in CH_2Cl_2 contained in 1.0 cm quarts cells. Measurements were carried out between 900 and 200 nm. Elemental analyses were carried out at the Institute of Chemistry, Academia Sinica.

Variable-temperature (4.2–300 K) magnetic susceptibility data were measured on compounds **1–5** with use of a Quantum Design Squid MPMS susceptometer maintained by the Physical Department at National Taiwan University. The susceptometer was operated at a magnetic field strength 10 KG for all compounds. Diamagnetic corrections were estimated from Pascal's constants and applied to the calculated molar paramagnetic susceptibilities. The values of correction for **1–5** are -2.429×10^{-4}, -2.726×10^{-4}, -3.023×10^{-4}, -3.023×10^{-4}, and -3.321×10^{-4} cm^3 mol^{-1}, respectively.

The single-crystal X-ray determinations of compounds **3–5** were carried out on an Enraf Nonius CAD4 diffractometer at 298 K. Absorption corrections were made with empirical ψ rotation for all three compounds. The X-ray crystal data are summarized in Table 1. Listings of the complete tables of bond distances and angles, thermal parameters, and observed and calculated structure factors of **3–5** are given as supplementary materials.

2.8. Structure determination of 3

A dark black crystal (0.25 × 0.19 × 0.13 mm), which was obtained when a layer of benzene was allowed to slowly diffuse into a CH_2Cl_2 solution of **3**, was used for data collection. Cell dimensions were obtained from 25 reflections with $14.55° < 2\theta < 34.28°$. The θ–2θ scan technique was used to record the intensities for all reflections for which $1° < 2\theta < 44.8°$. Of the 1164

Table 1
Experimetal and crystal data for the X-ray structures

Compounds	3	4	5
Formula	$C_{16}H_{18}FeI_3$	$C_{16}H_{18}FeI_3$	$C_{19}H_{22}FeI_3$
Crystal system	monoclinic	orthorhombic	orthorhombic
Space group	$C2/c$	$Pnma$	$Cmca$
a, Å	11.110(2)	8.699(1)	18.456(4)
b, Å	9.372(2)	13.461(2)	33.401(7)
c, Å	18.003(2)	15.747(3)	13.470(5)
β, deg	107.294(9)		
V, Å^3	1789.7(4)	1844.0(5)	8304 (4)
Z	4	4	16
f_W, g mol^{-1}	646.88	646.88	686.94
ρ_{calc}, g cm^{-3}	2.401	2.330	2.198
μ, mm^{-1}	5.96	5.78	41.28
λ, Å	0.71073	0.71073	1.54178
2θ, max	44.8	44.9	119.8
max, min trans. coef.	0.998, 0.849	1.000, 0.718	0.988, 0.385
R_F	0.033	0.041	0.077
R_{wF}	0.040	0.042	0.090

unique reflections, there were 962 with $F_0 > 2.0\sigma$ (F_0^2), where σ (F_0^2) were estimated from counting statistics. These data were used in the final refinement of the structural parameters.

A three-dimensional Patterson synthesis was used to determine the heavy-atom positions, which phased the data sufficiently well to permit location of the remaining non-hydrogen atoms from Fourier synthesis. All non-hydrogen atoms were refined anisotropically. H atoms were introduced in calculated positions (1.08 Å) and refined isotropically. The final positional parameters for all atoms can be found in Table 2, and the selected bond distances and angles are given in Table 3.

2.9. Structure determination of 4

A dark black crystal (0.29 × 0.31 × 0.28 mm) was obtained when a layer of hexane was allowed to diffuse slowly into a solution of CH_2Cl_2. Data were collected to a 2θ value of 44.9°. The unit cell dimensions were obtained from 25 reflections with 15.37° < 2θ < 34.44°. Of the 1270 unique reflections, there were 818 with $F_0 > 2.0\sigma$ (F_0^2). These data were used in the final refinement of structural parameters. Structure refinement was carried out in the same manner as described for **3**. Atomic coordinates and the selected bond dis-

Table 2
Atomic coordinates and thermal parameters (Å^2) for **3**

Atom	x	y	z	B_{iso} [a]
I1	0.50	0.14615(8)	0.25	4.16(5)
I2	0.40417(8)	0.14023(8)	0.08084(4)	6.81(4)
Fe	0.00	0.1957(2)	0.25	2.68(7)
C1	−0.1786(7)	0.1392(8)	0.1880(5)	3.4(4)
C2	−0.1802(7)	0.2801(9)	0.2147(5)	3.7(4)
C3	0.1343(7)	0.2824(8)	0.2037(5)	3.4(4)
C4	0.1021(7)	0.1404(8)	0.1769(5)	3.4(4)
C5	0.1348(7)	0.0509(8)	0.2443(5)	3.8(4)
C6	−0.2011(8)	0.089(1)	0.1059(5)	5.1(5)
C7	−0.107(1)	0.147(1)	0.0639(6)	5.9(5)
C8	0.0295(9)	0.094(1)	0.0957(5)	5.1(5)

[a] B_{iso} is the mean of the principal axes of thermal ellipsoid.

Table 3
Selected bond distances (Å) and bond angles (deg) for **3**

	Distance		
I(1)–I(2)	2.9126(8)	C(1)–C(6)	1.50(1)
Fe–C(1)	2.037(8)	C(2)–C(3)	1.40(1)
Fe–C(2)	2.069(7)	C(3)–C(4)	1.42(1)
Fe–C(3)	2.078(7)	C(4)–C(5)	1.43(1)
Fe–C(4)	2.043(7)	C(4)–C(8)	1.51(1)
Fe–C(5)	2.047(7)	C(6)–C(7)	1.55(1)
C(1)–C(2)	1.41(1)	C(7)–C(8)	1.54(1)
C(1)–C(5)	1.43(1)		
	Angle		
I(2)–I(1)–I(2) [a]	177.82(4)	C(2)–C(3)–C(4)	108.5(7)
C(2)–C(1)–C(5)	106.7(7)	C(3)–C(4)–C(5)	106.6(7)
C(1)–C(2)–C(3)	109.5(7)	C(1)–C(5)–C(4)	108.6(7)

[a] 1.000 − x y 0.500 − z.

Table 4
Atomic coordinates and thermal parameters (Å^2) for **4**

Atom	x	y	z	B_{iso} [a]
I1	0.01484(1)	0.75	0.32109(7)	4.66(6)
I2	0.0210(1)	0.53383(7)	0.32714(6)	6.16(5)
Fe	0.5602(3)	0.75	0.4714(1)	3.2(1)
C1	0.579(2)	0.8630(8)	0.5568(8)	4.6(6)
C2	0.690(2)	0.8783(9)	0.4903(8)	4.8(6)
C3	0.605(2)	0.8891(8)	0.4145(9)	5.1(7)
C4	0.449(2)	0.8784(9)	0.432(1)	5.9(8)
C5	0.429(2)	0.8626(8)	0.521(1)	5.3(7)
C6	0.623(2)	0.845(1)	0.6483(9)	8(1)
C7	0.282(2)	0.8442(1)	0.565(1)	9(1)
C8	0.714(3)	0.75	0.663(1)	10(2)
C9	0.210(2)	0.75	0.564(2)	8(2)

[a] B_{iso} is the mean of the principal axes of thermal ellipsoid.

Table 5
Selected bond distances (Å) and bond angles (deg) for **4**

	Distance		
I(1)–I(2)	2.912(1)	C(1)–C(6)	1.51(2)
Fe–C(1)	2.04(1)	C(2)–C(3)	1.41(2)
Fe–C(2)	2.08(1)	C(3)–C(4)	1.39(2)
Fe–C(3)	2.11(1)	C(4)–C(5)	1.44(2)
Fe–C(4)	2.08(1)	C(5)–C(7)	1.47(2)
Fe–C(5)	2.05(1)	C(6)–C(8)	1.52(2)
C(1)–C(2)	1.44(2)	C(7)–C(9)	1.42(2)
C(1)–C(5)	1.42(2)		
	Angle		
I(2)–I(1)–I(2) [a]	175.68(5)	C(2)–C(3)–C(4)	110(1)
C(2)–C(1)–C(5)	109(1)	C(3)–C(4)–C(5)	109(1)
C(1)–C(2)–C(3)	106(1)	C(1)–C(5)–C(4)	106(1)

[a] x 1.500 − y z.

Table 6
Atomic coordinates and thermal parameters (Å^2) for **5**

Atom	x	y	z	B_{iso} [a]
I1	0.25	0.42883(8)	0.25	4.2(1)
I2	0.2306(1)	0.42840(9)	0.0364(2)	6.5(1)
I3	0	0.24608(9)	0.9978(3)	3.7(1)
I4	0	0.1639(1)	1.0708(4)	6.9(2)
I5	0	0.3273(1)	0.9236(4)	7.8(2)
Fe1	0.25	0.2460(2)	0.25	2.4(2)
Fe2	0	0.4954(2)	0.2501(6)	2.8(2)
C1	0.200(2)	0.2790(9)	0.142(2)	4(2)
C2	0.278(2)	0.2787(8)	0.129(2)	4(1)
C3	0.301(2)	0.2347(9)	0.122(2)	5(2)
C4	0.239(2)	0.2095(8)	0.131(2)	5(2)
C5	0.177(1)	0.2351(9)	0.141(3)	5(2)
C6	0	0.471(2)	0.104(5)	6(3)
C7	0.063(2)	0.500(1)	0.128(2)	4(2)
C8	0.037(2)	0.5404(2)	0.162(2)	4(1)
C9	0	0.448(1)	0.340(3)	4(2)
C10	0.062(2)	0.4707(8)	0.358(2)	4(1)
C11	0.041(1)	0.5135(9)	0.385(2)	4(1)
C12	0.154(2)	0.311(1)	0.168(3)	7(2)
C13	0.120(2)	0.3082(9)	0.274(4)	8(3)
C14	0.327(2)	0.311(1)	0.139(3)	6(2)
C15	0.241(3)	0.167(1)	0.154(4)	9(3)
C16	0.25	0.148(2)	0.25	19(8)
C17	0	0.430(1)	0.099(4)	6(3)
C18	0	0.403(2)	0.179(7)	12(6)
C19	0	0.409(1)	0.288(4)	8(4)
C20	0.086(2)	0.570(1)	0.202(3)	6(2)
C21	0.131(2)	0.555(1)	0.295(3)	6(2)
C22	0.087(2)	0.549(1)	0.391(2)	5(2)

[a] B_{iso} is the mean of the principal axes of thermal ellipsoid.

tances and angles are given in Tables 4 and 5, respectively.

2.10. Structure determination of 5

A dark black crystal (0.25 × 0.19 × 0.22 mm) was obtained following the same procedure as for **4**. Data were collected to a 2θ value of 119.8°. The cell dimensions were obtained from 25 reflections with 2θ in the range 16.08°–44.01°. Of the 3191 unique reflections, there were 1832 with $F_0 > 2.0\sigma$ (F_0^2). These data were used in the final refinement of the structural parameters.

Structure refinement was carried out in the same manner as described for **3**. Atomic coordinates are given in Table 6, and the selected bond distances and angles are given in Table 7.

3. Results

3.1. Molecular structure of 3

Compound **3** crystallizes in the monoclinic space group $C2/c$. Fig. 1 shows the molecular structure and

Table 7
Selected bond distances (Å) and bond angles (deg) for **5**

	Distance		
I(1)–I(2)	2.899(3)	Fe(2)–C(10)	2.03(3)
I(3)–I(4)	2.916(5)	C(1)–C(2)	1.45(4)
I(3)–I(5)	2.892(5)	C(1)–C(5)	1.53(4)
Fe(1)–C(1)	2.04(3)	C(2)–C(3)	1.54(4)
Fe(1)–C(2)	2.03(3)	C(3)–C(4)	1.43(5)
Fe(1)–C(3)	2.01(3)	C(4)–C(5)	1.44(5)
Fe(1)–C(4)	2.03(3)	C(6)–C(7)	1.56(5)
Fe(1)–C(5)	2.03(3)	C(7)–C(8)	1.49(5)
Fe(2)–C(6)	2.13(6)	C(8)–C(8) [b]	1.36(6)
Fe(2)–C(7)	2.03(3)	C(9)–C(10)	1.40(4)
Fe(2)–C(8)	2.04(3)	C(10)–C(11)	1.52(4)
Fe(2)–C(9)	1.99(4)	C(11)–C(11) [b]	1.50(5)
	Angle		
I(2)–I(1)–I(2) [a]	179.4(1)	C(2)–C(1)–C(5)	106(2)
I(4)–I(3)–I(5)	179.5(2)	C(1)–C(2)–C(3)	107(2)
C(3)–C(4)–C(5)	107(2)	C(2)–C(3)–C(4)	109(3)
C(1)–C(5)–C(4)	110(2)	C(10)–C(9)–C(10) [b]	109(3)
C(7)–C(6)–C(7) [b]	96(3)	C(9)–C(10)–C(11)	110(2)
C(6)–C(7)–C(8)	112(3)	C(10)–C(11)–C(11) [b]	105(2)
C(7)–C(8)–C(8) [b]	109(2)		

[a] 0.500 − x y 0.500 − z.
[b] − x y z.

atomic labeling scheme for cation and triiodide anion. As shown in Fig. 1, the two Cp rings are nearly eclipsed with an average staggering angle of 1.0(3)°, and the Fe–C distances range from 2.037(8) Å to 2.078(7) Å. The spread of Fe–C distances is a result of the non-parallel Cp rings where the angle between the two least-squares rings is 14.3(3)°. The average of these Fe–C distances, i.e. 2.055(7) Å, lies midway between the 2.045 Å observed for ferrocene [15] and 2.075 Å

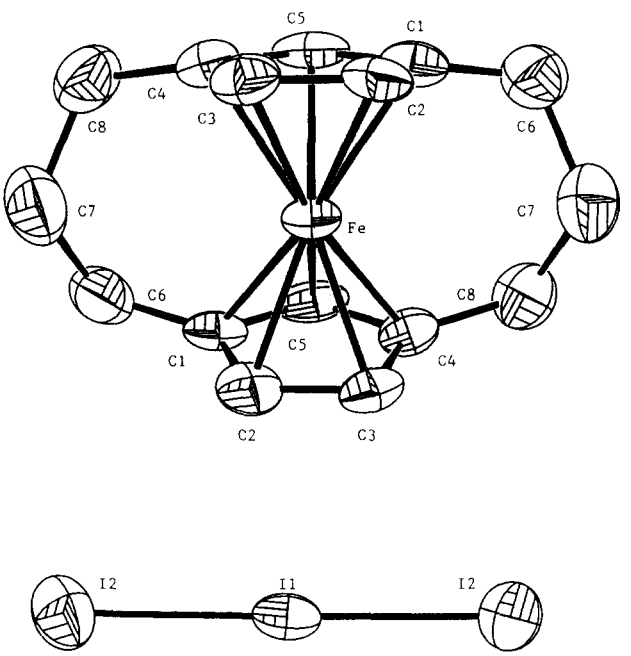

Fig. 1. ORTEP drawing for **3** with 30% thermal ellipsoids.

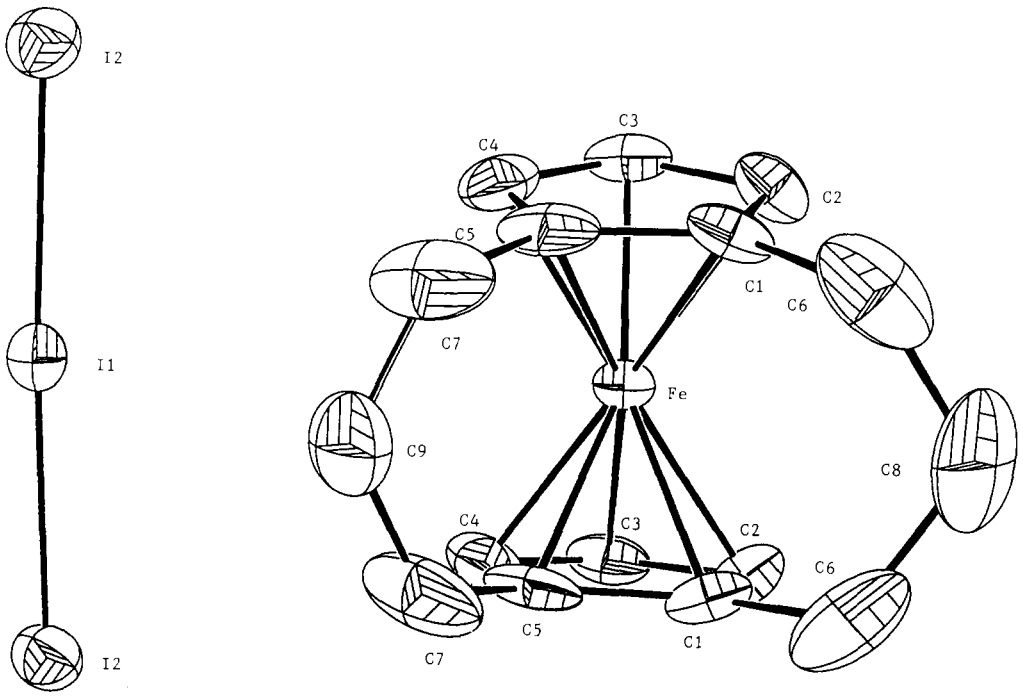

Fig. 2. ORTEP drawing for **4** with 30% thermal ellipsoids.

observed for the ferrocenium cation [16]. Inspection of the iron to Cp rings distances shows that both distances (1.661(4) Å and 1.662(1) Å) are also intermediate between the analogous values for neutral ferrocene (1.65 Å) and the ferrocenium ion (1.70 Å). A direct comparison is made between **3** and related molecules (Table 8).

The triiodide anion sits on a center of inversion. The I(1)–I(2) bond length is 2.9126(8) Å, which compares well with other determinations of the symmetric triiodide bond length [10,14]. The triiodide is nearly linear as required by the inversion symmetry.

3.2. Molecular structure of 4

An ORTEP plot of cation **4** and the triiodide anion are given in Fig. 2. The results of our crystallographic

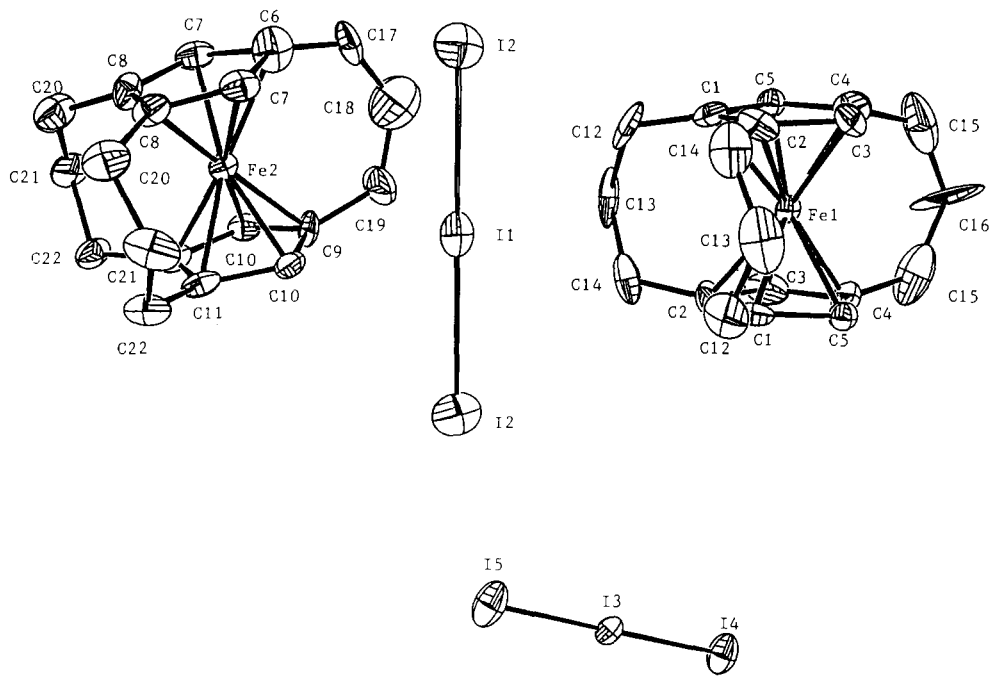

Fig. 3. ORTEP drawing for **5** with 30% thermal ellipsoids.

study at 298 K show that the cation **4** crystallizes in the orthorhombic space group *P*nma. Both cation and anion lie on a crystallographic mirror plane. Average distances from the iron atom to the Cp ring center atoms are 2.073 Å. This distance is closer to the value of 2.075 Å found for the ferrocenium cation [16] than the value of 2.045 Å found for ferrocene [15]. The distance from the iron to the Cp ring is 1.684(7) Å. The tilt angle between the two least-squares rings is 9.2(6)°. A direct comparison is also made between **4** and related molecules (see Table 8).

The distance of I–I in symmetric triiodide is 2.912(1) Å, which is in accord with the standard value of 2.920 Å proposed for the centrosymmetric triiodide ion [17]. The bond angle (I(2)–I(1)–I(2)) of the non-linear triiodide anion is 175.68(5)°.

3.3. Molecular structure of 5

Compound **5** crystallizes in the orthorhombic space group *C*mca. There are two crystallographically independent molecules in the unit cell, and the molecular structures and atomic labeling schemes for cations and the triiodide anion are shown in Fig. 3. The cation associated with Fe(1) is located about a two-fold axis and the cation associated with Fe(2) lies on a crystallographic mirror plane. As shown in Fig. 3, the two Cp rings in each ferrocenium cation are nearly eclipsed, 0.3° and 2.1° associated with Fe(1) and Fe(2), respectively. In comparison with cations **3** and **4**, the two Cp rings in each ferrocenium cation are more parallel. The angles between the two least-squares rings of $Fe_1(Cp)_2$ and $Fe_2(Cp)_2$ are 3.90° and 4.96°, respectively. Furthermore, the average value of Fe–C distances and the average distance from the Fe ion to Cp ring are 2.035(3) Å and 1.602(12) Å, respectively. These values are significantly shorter than the corresponding values observed for ferrocene [15] and ferrocenium cation [16]. From this comparison, we can conclude that the interannular tri-trimethylene bridges squeeze the Fe atom.

There are also two independent triiodide anions in the unit cell. The I–I distance in the linear and symmetric I(2)–I(1)–I(2) anion is 2.899(3) Å which agrees well with the value of 2.920 Å for symmetric triiodide anion [17]. The I(4)–I(3)–I(5) anion is asymmetric and has a slight I_2–I^- character, where I(3)–I(4) = 2.916(5) Å and I(3)–I(5) = 2.892(5) Å. From the I–I bond distances, we can conclude that the I(4) atom carries more negative charge.

Table 8
Comparison of the interatomic distances (Å) and tilt angles (deg)

Compound	Fe–C	Fe–Cp	Tilt angle
1 [a]	2.075	1.70	
2 [a]	2.074(3)	1.67	13.2
3	2.055(7)	1.662(3)	14.3(3)
4	2.073(1)	1.684(7)	9.2(6)
5 [b]	2.028(3)	1.592(3)	3.9(1)
	2.044(3)	1.613(2)	4.96(2)

[a] From ref. [19].
[b] Two independent molecules in one unit cell.

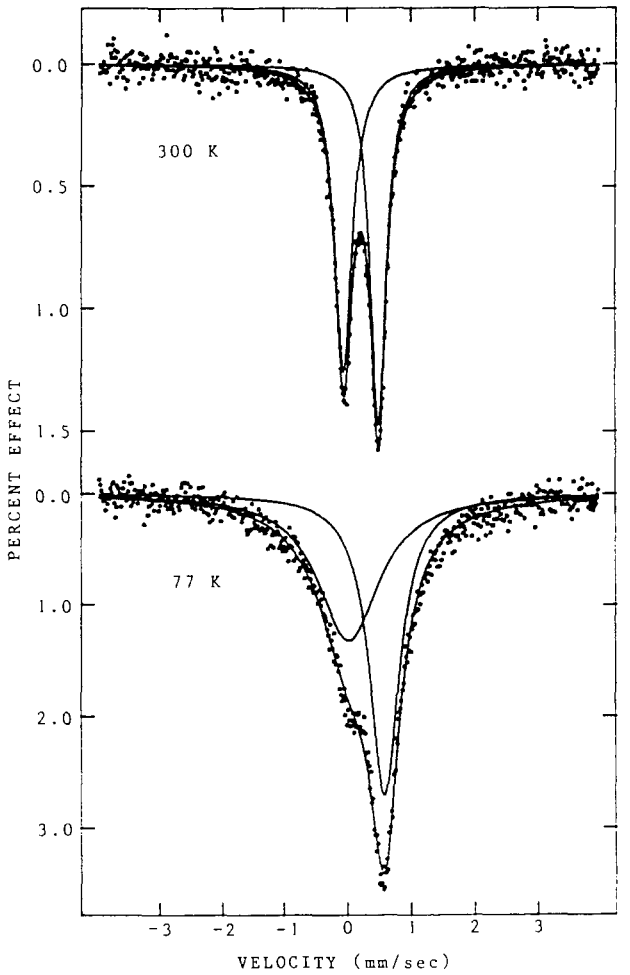

Fig. 4. ^{57}Fe Mössbauer spectra of **3** at 300 K (top) and 77 K (bottom).

3.4. ^{57}Fe Mössbauer characteristics

As shown in Figs. 4–6, the ^{57}Fe Mössbauer spectra were run at 300 K and 77 K for compounds **3–5**. The absorption peaks in each spectrum were fitted by least-squares to Lorentzian lines and the resulting fitting parameters are summarized in Table 9, together with data for related ferrocenium cations. Surprisingly, an unusually large quadrupole splitting (ΔE_Q) is seen in the Mössbauer spectra of **3–5** at 300 K and 77 K. The ΔE_Q values of **3–5** are 0.541, 0.936, and 0.627 mm s^{-1} at 300 K, respectively. As mentioned in the introduction, the ^{57}Fe Mössbauer spectra of the ferrocenium cations (electronic ground state $^2E_{2g}$) are characterized by small or vanishing quadrupole splitting [18,19]. To our knowledge, compounds **3–5** are the first mononuclear ferrocenium compounds to show such

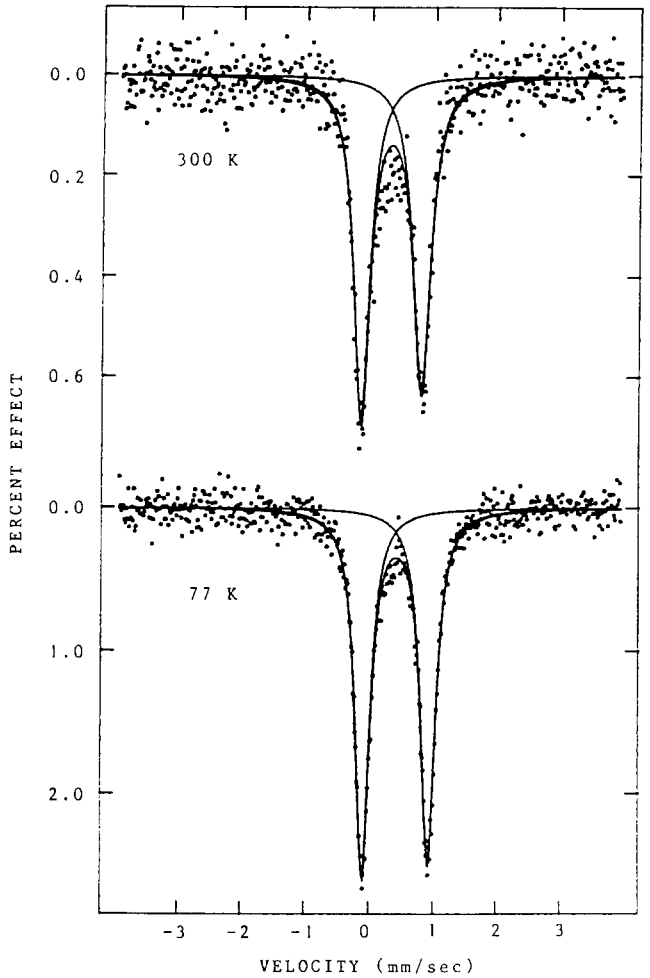

Fig. 5. ^{57}Fe Mössbauer spectra of **4** at 300 K (top) and 77 K (bottom).

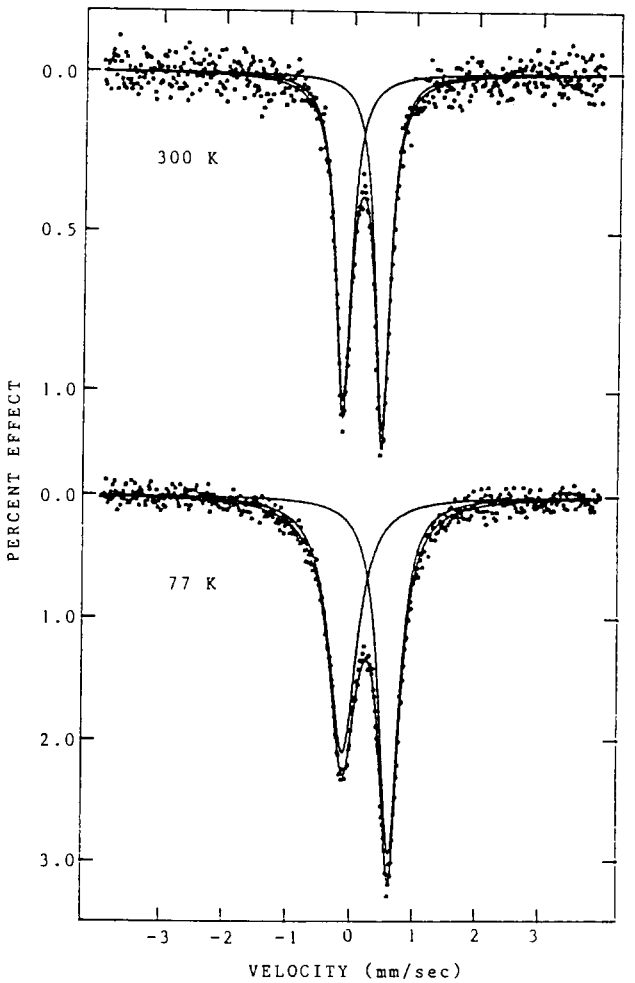

Fig. 6. ^{57}Fe Mössbauer spectra of **5** at 300 K (top) and 77 K (bottom).

unusually large quadrupole splitting at room temperature. The ^{57}Fe Mössbauer data for compounds **1–5** were also collected at 77 K. Selected spectra are also shown in Figs. 4–6, and the complete set of fitting parameters are also listed in Table 9. The values of quadrupole splitting for compounds **3–5** are 0.556, 1.023, and 0.740 mm s^{-1} at 77 K.

3.5. Magnetic susceptibility measurements

The room-temperature moments of **2–5** range from about 2.08–2.6 BM. The deviation from the spin-only value of 1.73 BM establishes that compounds **2–5** have a $^2E_{2g}$ ground state as found [4] for compound **1**, and shows that the low-symmetry distortion is not so large. If the distortion was so large, the orbital contribution to the magnetic moment would be quenched leaving an essentially spin-only value for effective moment.

Variable-temperature magnetic susceptibility studies (μ_{eff} vs. T) in the range of 5–300 K are shown in Figs. 7 and 8. It is clear from these figures, that not all five μ_{eff} vs. T curves have essentially the same shape. In comparison with ferrocenium triiodide, the interannular trimethylene bridge substitution in **2** and **4** has the effect only of displacing the curve to higher effective magnetic moment. In the case of **3** and **5**, we find that

Table 9
^{57}Fe Mössbauer least-fitting parameters

Compound	T(K)	ΔE_Q [a]	δ [b]	Γ [c]
1 [d]	300	0.156	0.417	0.646, 0.338
	120	0.245	0.442	1.422, 0.508
2 [e]	300	0.148	0.382	0.472, 0.314
3	300	0.541	0.321	0.332, 0.298
	77	0.556	0.404	1.168, 0.568
4	300	0.936	0.425	0.312, 0.341
	77	1.023	0.514	0.274, 0.285
5	300	0.627	0.256	0.309, 0.282
	77	0.738	0.347	0.533, 0.382

[a] Quadrupole-spitting in mm s^{-1}.
[b] Isomer shift referenced to iron foil in mm s^{-1}.
[c] Full width at half-height taken from the least-squares-fitting program. The width for the line at more negative velocity is listed for first each doublet.
[d] From ref. [18].
[e] From ref. [19].

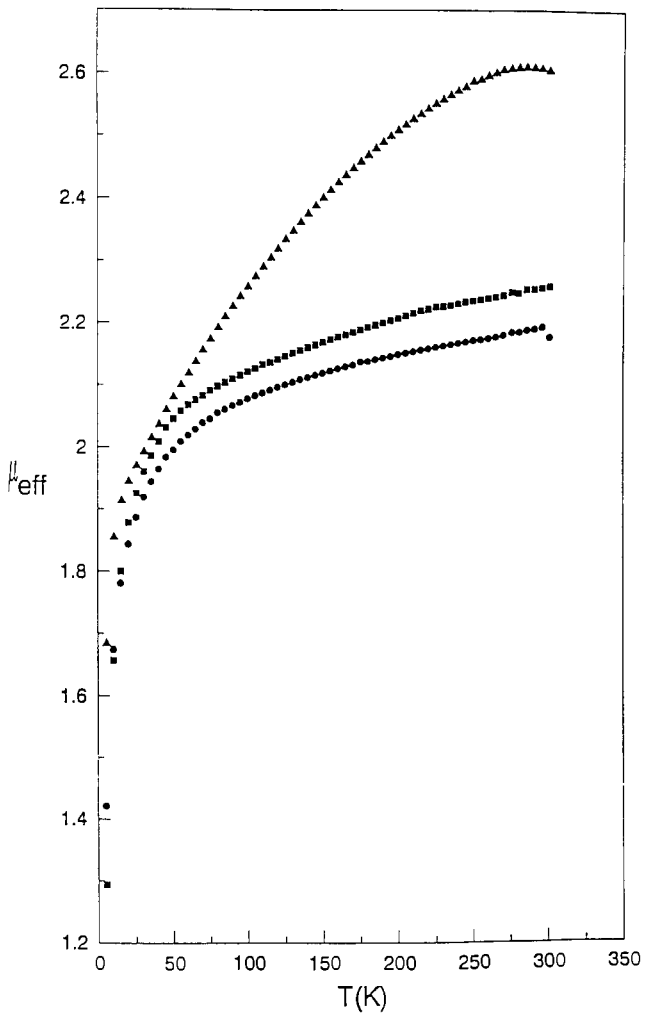

Fig. 7. Variable-temperature magnetic susceptibility of **1** (●), **2** (■), and **4** (△).

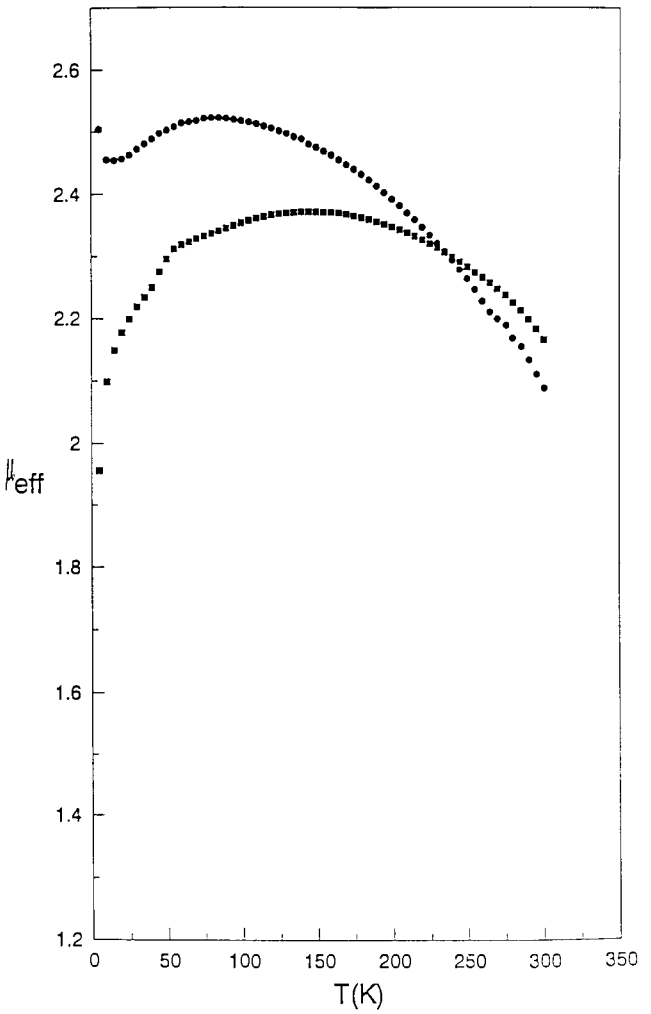

Fig. 8. Variable-temperature magnetic susceptibility of **3** (●) and **5** (■).

the μ_{eff} approaches to a maximum and then becomes small as temperature becomes small.

3.6. Electronic spectra

The absorption spectrum of ferrocenium ion has been investigated by several groups. Sohn et al. reported [20] that a 10 M LiCl aqueous solution of ferrocenium BF_4 exhibits four bands and at least four shoulders at 617 (450), 564 (250), 523 (190), 467 (150), 380 (350), 283 (9700), 250 (16000), and 198 nm (14000 cm^{-1} M^{-1}). Ring substitution and temperature effects were used to assign the first band (617 nm) to the ligand-to-metal $^2E_{2g} \rightarrow {}^2E_{1u}$ transition [20]. The four shoulders at 564, 523, 467, and 380 nm were assigned as essentially metal d–d transitions. Of particular interest to the work of Sohn et al. is that the $^2E_{2g} \rightarrow {}^2E_{1u}$ charge transfer band in the visible region exhibits vi-

Table 10
The ultraviolet and visible spectra of **1–5** in CH_2Cl_2

Compound	λ_{max} [a], (ϵ: cm^{-1} M^{-1})	
1	224(17806),	291(9232), 363(4431), 502(1484),
2	224(14523), 252(6169),	292(22594), 364(11772), 500(sh, 1120), 600(sh, 303)
3	224(14887), 246(10997),	293(30953), 365(17094), 496(sh, 802), 692(225)
4	223(12543), 258(12426),	293(44394), 365(23431), 500(728), 625(sh, 381)
5	223(14677), 238(10983),	294(30174), 365(16714), 500(sh, 859), ~750 [b]

[a] In nanometres.

[b] Vibrational structure of this band can be seen at 708(355), 725(383), 745(overlap with 754, 381), 754(overlap with 745, 381), 775(402), and 796 nm (346 cm^{-1} M^{-1}).

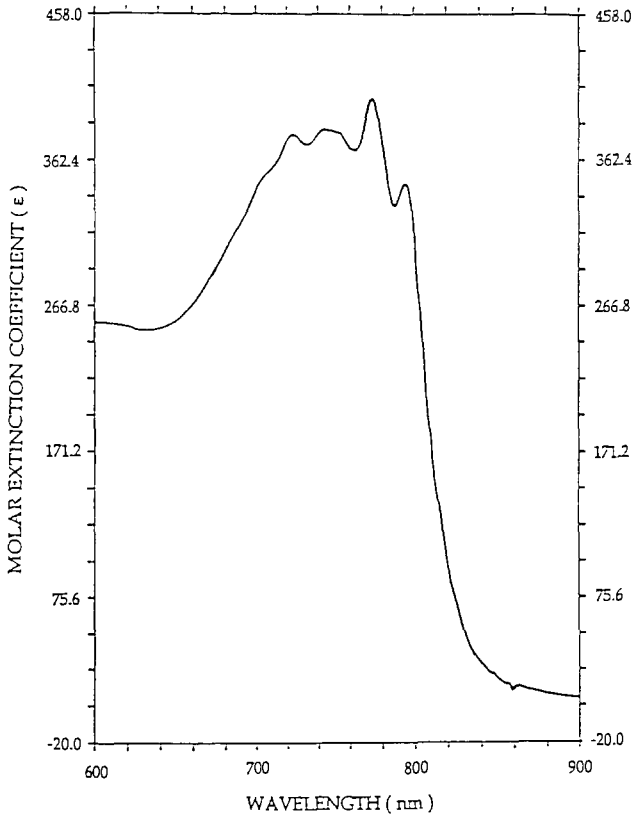

Fig. 9. Vibrational structure of approximately the 750 nm band for **5** in CH_2Cl_2 solution at room temperature.

brational structure at low temperatures. The observed vibrational progression was assigned to the symmetric ring-metal stretching frequency. In this section we will show how absorption spectroscopy applied to compounds **1–5** will give information as to the location and character of various excited states.

The band positions and intensities of compounds **1–5** in CH_2Cl_2 solution are given in Table 10. Sohn et al. [20] and Prins [21] have shown that the $^2E_{2g} \rightarrow {}^2E_{1u}$ transition shifts significantly upon ring substitution, and on this basis assigned it as ligand-to-metal charge transfer. Our studies of the substitutional behavior of this transition are in accord with these of Sohn et al. and Prins. As shown in Table 10, the 600 nm absorption of **2** in a solution of CH_2Cl_2 undergoes a red shift upon trimethylene interannular bridge substitution. Thus this band appears at 692 nm and 625 nm for **3** and **4**, respectively, and shows a dramatic shift to 750 nm for **5** at room temperature. Since all of the interannular bridges are trimethylene alkylations, the observed shift to lower energy is in qualitative agreement with the assigned ligand-to-metal charge-transfer character of the transition.

It is interesting to find that the vibrational progressions can also be seen at room temperature for compound **5**. To our knowledge, compound **5** is the first ferrocenium compound to show vibrational progressions at room temperature. As illustrated in Fig. 9, compound **5** seemingly has five clear vibrational components at 708 (sh), 725, 745 (overlap), 754 (overlap), and 796 nm. Furthermore, the spacing between each component is not equal and this could be a result of the splitting of the $^2E_{1u}$ excited state by components of the low-symmetry crystal field. As reported by Prins [22], the $^2E_{2g}$ ground state of the ferrocenium ion is split into two Kramer doublets by the combined action of the spin-orbital interaction and a low-symmetry perturbation. In the studies of absorption spectra of ferrocenium ions, Sohn et al. found [20] that the vibrational structure of ferrocenium trichloroacetate at 77 K is most likely a progression of doublets. To explain the vibrational structure of ferrocenium trichloroacetate, Sohn et al. also proposed [20] that the $^2E_{1u}$ excited state could be also split by the low-symmetry crystal field. The low-symmetry distortion parameter of the $^2E_{1u}$ excited state was estimated [20] as 140 cm^{-1}. In our case the two electronic origins are not easy to locate. If the first two components at 796 nm and 775 nm are taken as the two origins, the distortion in the excited state is estimated as 340 cm^{-1}. It seems that the first progression with an origin at 796 nm has a lower intensity than the second progression. Further study of this absorption band at low temperature may be helpful in better understanding the vibration structure.

Compounds **2–5** also exhibit one low-intensity band at approximately 500 nm. This band appears at the same position in the series of ferrocenium salts. The intensity and position are nearly insensitive to the interannular bridge substitution. Therefore, this band may be assigned as metal d–d transition.

4. Discussion

In the theory there are two possible explanations for the observation of unusually large quadrupole splitting in compounds **3–5**. First, a thermal population of the $^2A_{1g}(a_{1g}{}^1e_{2g}^4)$ state would have the desired effect. The energy difference $\Delta E(^2A_{1g} - {}^2E_{2g})$ in ferrocenium cation is estimated [20] to be relative small (approximately 400 cm^{-1}). Our magnetic measurements indicate that compounds **1–5** have the orbitally degenerate $^2E_{2g}(a_{1g}{}^2e_{2g}^3)$ ground-state configuration. Furthermore, the observed temperature independence of the effective magnetic moments for **3** and **5** is explicable in terms of a thermal population of the $^2A_{1g}$ state. As pointed out by Hendrickson et al. [2], theoretically the effective magnetic moment decreases with increasing low-symmetry distortion. Furthermore, μ_{eff} should linearly increase with increasing temperature. However, experimentally the magnetic moments for ferrocenium

ions are found [2] to be relatively temperature independent in the range of 40–300 K, for instance, ferrocenium hexafluorophosphate, tetrafluoroborate, and triiodide salts reported by Hendrickson et al.. The observed temperature independence of the effective magnetic moments for these ferrocenium salts is explained in terms of either a temperature-dependent low-symmetry crystal field distortion or thermal population of the $^2A_{1g}(a_{1g}{}^1e_{2g}^4)$ state. Our compounds (**3** and **5**) provide a good example to elucidate the presence of thermal population of the $^2A_{1g}$ state. Thermal population of $^2A_{1g}$ state will dramatically affect the shape of the μ_{eff} vs. T curve. If this state becomes thermally populated at room temperature, the μ_{eff} could approach to a maximum and then become small as temperature decreases. Theoretically μ_{eff} for the $^2A_{1g}$ state should approach the spin-only value of 1.73 BM. In comparison with the $^2E_{2g}$ electronic state, the $^2A_{1g}$ state has a larger electric field gradient which can induce a larger quadrupole splitting.

Secondly, we propose that the larger ΔE_Q value is mainly a result of the metal non-bonding orbitals ($d_{x^2-y^2}$, d_{xy}) starting to interact with the ligand π orbitals as the Cp rings are bent back. For ferrocene it was found that the three highest filled and the two lowest empty orbitals are for the greater part localized on the metal atom and that the energetic order of the orbitals is e_{1g} (d_{xz}, d_{yz}) > $a_{1g}(d_{z^2})$ > $e_{2g}(d_{x^2-y^2}, d_{xy})$ [22]. A value of approximately 3 ev has been found for the energy difference between the e_{1g} and a_{1g} [23]. For the orbitals energy difference between the a_{1g} and e_{2g} a value of 0.5 ev has been obtained from an analysis of the absorption spectrum [22]. Lauher and Hoffmann [24] have derived the fragment orbitals for a bent $M(Cp)_2$ unit from the parallel geometry. For detailed information concerning the reactivities and general features of $M(Cp)_2$ fragments, one should refer to the original works. Bending back the Cp rings splits the e_{2g} set into orbitals of $1a_1(d_{x^2-y^2})$ and $b_2(d_{xy})$ symmetry. The highest filled a_{1g} orbital rises rapidly in energy as the Cp rings are bent back. The a_{1g} combination of Cp π orbitals has a greater overlap with metal d_{z^2} at a bent geometry. Some metal s character and $d_{x^2-y^2}$ from $1a_1$ mix with what was a_{1g}, so that the torus of d_{z^2} becomes hybridized away from the Cp ligands. As mentioned previously the electronic ground state of the ferrocenium ion is a doublet, $^2E_{2g}(a_{1g}{}^2e_{2g}^3)$ [22]. The order and character of the highest filled and lowest empty orbitals in ferrocenium ion have been found to be: $e_{1g}(d_{xz}, d_{yz})$ > $e_{2g}(d_{x^2-y^2}, d_{xy})$ > $a_{1g}(d_{z^2})$ [22]. As shown in Fig. 10, bending back the Cp rings for a ferrocenium ion splits the highest filled e_{2g} set into $b_2(d_{xy})$ and $2a_1$ ($d_{x^2-y^2}$) orbitals. We propose that the $2a_1(d_{x^2-y^2})$ orbital rises rapidly in energy as the Cp rings are bent back. This is partly a result of the avoided crossing with $1a_1$ and the fact that some s

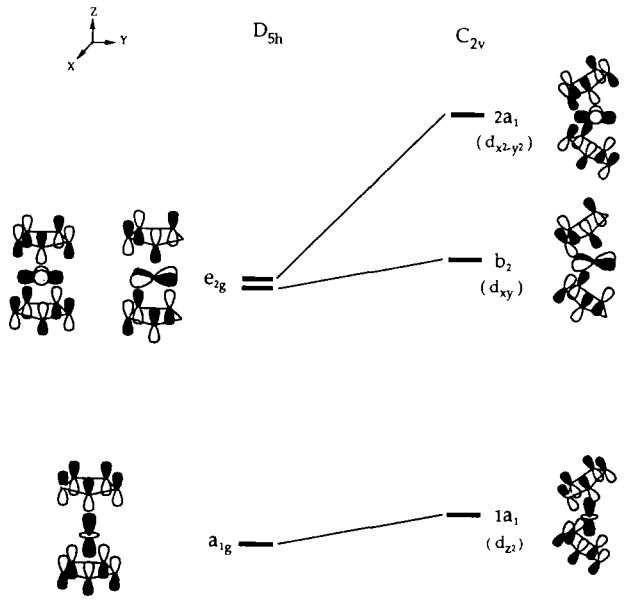

Fig. 10. Fragment orbitals for bending ferrocenium ion from parallel geometry.

character and d_{z^2} from $1a_1$ mix into $2a_1$. The mixing between $1a_1$ and $2a_1$ serves to keep $1a_1$ at constant energy. Thus, the a_1 combination of Cp π levels has a greater interaction with metal $d_{x^2-y^2}$ at a bent geometry. As indicated by low-temperature electronic absorption, it has been reported [1] that the Cp rings in the cation of **2** are tilted and because of the bending of the rings the $e_{2g}(d_{x^2-y^2}, d_{xy})$ metal orbitals take part in bonding to the ring. In the case of ferrocenium cation, no e_{2g} orbital participation in metal-ring bonding is found. We suggest that the greater the bonding between the $2a_1(d_{x^2-y^2})$ orbital and Cp rings the greater the probability for electron density on the $2a_1$. Under these circumstances the iron ions lose some degree of their Fe(III) character, and this results in an increase in the quadrupole splitting of ^{57}Fe Mössbauer spectrum because the iron ions are closer to Fe(II) in their properties. This is what we observe for compounds **2–5** in the studies of ^{57}Fe Mössbauer.

5. Concluding comments

In this paper, we show that minor perturbations caused by the interannular trimethylene bridge have pronounced effects on the electronic structure. To have a qualitative explanation for the unusually large quadrupole splitting in the ^{57}Fe Mössbauer spectra, we suggest that the metal non-bonding orbitals ($d_{x^2-y^2}$, d_{xy}) start to interact with the ligand π orbitals as the Cp rings of ferrocenium ion are bent back. The ^{57}Fe Mössbauer results indicate that the ordering of the metal ($d_{x^2-y^2}$, d_{xy})-ligand interaction is **4** > **5** > **3** > **2**

≈ 1. The tilt angles between the two least-squares Cp rings in **1–5** are approximately 0.0, 13.2, 14.3, 9.2, and 4.5°, respectively. Thus, there is a maximum metal ($d_{x^2-y^2}$, d_{xy})-ligand interaction as the two Cp rings tilt by about 9.2°. The studies of counter ion effects in the series of ferrocenium cations could further elucidate the correlation between the tilt angle and metal–ligand interaction. We believe that the interaction between cation and anion in the series of ferrocenium cations can also play an important role in determining the degree of tilting of the Cp rings from geometry. The counter ion will serve as a very sensitive probe of the state of electronic structure.

6. Supplementary material available

All complete tables of atomic coordinates and bond distances and angles for **3–5** (10 pages), tables of thermal parameters for **3**, **4**, and **5**, tables of observed and calculated structure factors for the same three compounds (20 pages) are available from the authors.

Acknowledgment

Acknowledgments are made to the National Science Council, Taiwan, ROC, and the Department of Chemistry at National Sun Yat-sen University for financial support.

References

[1] D.M. Duggan and D.N. Hendrickson, *Inorg. Chem.*, *14* (1975) 955.
[2] D.N. Hendrickson, Y.S. Sohn and H.B. Gray, *Inorg. Chem.*, *10* (1971) 1559.
[3] A. Horsfield and A. Wassermann, *J. Chem. Soc.*, *A*, (1970) 3202.
[4] R. Prins and A. Kortbeek, *J. Organomet. Chem.*, *33* (1971) C33.
[5] A. Horsfield and A. Wassermann, *J. Chem. Soc.*, *A*, (1972) 187.
[6] (a) M. Rosenblum, *Chemistry of the Iron Group Metallocenes*, Wiley-Interscience, NY, 1965; (b) D.A. Brown, *Transition Metal Chem.*, *3* (1966) 36; (c) C.J. Ballhausen and H.B. Gray, in A.E. Martell (ed.) *Chemistry of the Coordination Compounds*, Vol. I, Van Nostrand-Reinhild, 1971, Ch. 1.
[7] T.-Y. Dong and C.Y. Chou, *J. Chem. Soc., Chem. Commun.*, (1990) 1332.
[8] T.-Y. Dong, T.Y. Lee and H.M. Lin, *J. Organomet. Chem.*, *427* (1992) 109.
[9] T.-Y. Dong, T.Y. Lee, Y.S. Wen, S.H. Lee, C.F. Hsieh, G.H. Lee and S.M. Peng, *J. Organomet. Chem.*, *456* (1993) 239.
[10] T.-Y. Dong, D.N. Hendrickson, K. Iwai, M.J. Cohn, S.J. Geib, A.L. Rheingold, H. Sano, I. Motoyama and S. Nakashima, *J. Am. Chem. Soc.*, *107* (1985) 7996.
[11] K.L. Rinehart, D.E. Bublitz and D.H. Gustafson, *J. Am. Chem. Soc.*, *85* (1963) 970.
[12] T.D. Turbit and W.E. Watts, *J. Organomet. Chem.*, *46* (1972) 109.
[13] W. Crawford, T.D. Turbit and W.E. Watts, *J. Organomet. Chem.*, *105* (1976) 341.
[14] T.-Y. Dong, C.C. Schei, M.Y. Hwang, T.Y. Lee, S.K. Yeh and Y.S. Wen, *Organometallics*, *11* (1992) 573.
[15] P. Seiler and J.D. Dunitz, *Acta Crystallogr., Sect. B*, *35* (1979) 1068.
[16] N.J. Mammano, A. Zalkin, A. Landers and A.L. Rheingold, *Inorg. Chem.*, *16* (1977) 297.
[17] I. Runsink, S. Swen-Walstra and T. Migchelsen, *Acta Crystallogr., Sect. B*, *28* (1972) 1331.
[18] M.F. Moore, S.R. Wilson, M.J. Cohn, T.-Y. Dong, U.T. Mueller-Westerhoff and D.N. Hendrickson, *Inorg. Chem.*, *24* (1985) 4559.
[19] T.-Y. Dong, H.M. Lin, M.Y. Hwang, T.Y. Lee, L.H. Tseng, S.M. Peng and G.H. Lee, *J. Organomet. Chem.*, *414* (1991) 227.
[20] Y.S. Sohn, D.N. Hendrickson and H.B. Gray, *J. Am. Chem. Soc.*, *93* (1971) 3603.
[21] R. Prins, *J. Chem. Soc., Chem. Commun.*, (1970) 280.
[22] R. Prins, *Mol. Phys.*, *19* (1970) 603.
[23] (a) R. Prins and J.D.W. van Voorst, *J. Chem. Phys.*, *49* (1968) 4665; (b) D.R. Scott and R.S. Becker, *J. Organomet. Chem.*, *4* (1965) 409.
[24] J.W. Lauher and R.J. Hoffmann, *J. Am. Chem. Soc.*, *98* (1976) 1729.